Public Health England

NHS

NHS Breast Screening Programme Equipment Report 1601

Technical evaluation of Fujifilm AMULET Innovality digital mammography system

February 2017

Public Health England leads the NHS Screening Programmes

About Public Health England

Public Health England exists to protect and improve the nation's health and wellbeing, and reduce health inequalities. It does this through world-class science, knowledge and intelligence, advocacy, partnerships and the delivery of specialist public health services. PHE is an operationally autonomous executive agency of the Department of Health.

Public Health England, Wellington House, 133-155 Waterloo Road, London SE1 8UG
Tel: 020 7654 8000 www.gov.uk/phe
Twitter: @PHE_uk Facebook: www.facebook.com/PublicHealthEngland

About PHE Screening

Screening identifies apparently healthy people who may be at increased risk of a disease or condition, enabling earlier treatment or better informed decisions. National population screening programmes are implemented in the NHS on the advice of the UK National Screening Committee (UK NSC), which makes independent, evidence-based recommendations to ministers in the four UK countries. The Screening Quality Assurance Service ensures programmes are safe and effective by checking that national standards are met. PHE leads the NHS Screening Programmes and hosts the UK NSC secretariat.

PHE Screening, Floor 2, Zone B, Skipton House, 80 London Road, London SE1 6LH
www.gov.uk/topic/population-screening-programmes
Twitter: @PHE_Screening Blog: phescreening.blog.gov.uk

Prepared by: CJ Strudley, JM Oduko, KC Young
For queries relating to this document, please contact: phe.screeninghelpdesk@nhs.net
The image on page 8 is courtesy of Fujifilm.

Published February 2017
PHE publications gateway number: 2016633

About this document

Acknowledgements

The authors are grateful to the staff at the Breast Unit at Barnsley Hospital, for their cooperation in the evaluation of the system at their site.

Document Information	
Title	Technical evaluation of Fujifilm AMULET Innovality digital mammography system
Policy/document type	Equipment Report 1601
Electronic publication date	February 2017
Version	1
Superseded publications	None
Review date	None
Author/s	CJ Strudley, JM Oduko, KC Young
Owner	NHS Breast Screening Programme
Document objective (clinical/healthcare/social questions covered)	To provide an evaluation of this equipment's suitability for use within the NHSBSP
Population affected	Women eligible for routine and higher-risk breast screening
Target audience	Physicists, radiographers, radiologists
Date archived	Current

Contents

Executive summary

The purpose of the evaluation was to determine whether the Fujifilm AMULET Innovality meets the main standards in the NHS Breast Screening Programme (NHSBSP) and European protocols, and to provide performance data for comparison against other systems.

For use in the NHSBSP, it is recommended that the system is operated with the automatic exposure control (AEC) in iAEC mode at dose setting H (High). This allows image quality to approach or exceed the achievable level of image quality at all breast thicknesses. Operation at dose setting N (Normal) gives achievable image quality only for equivalent breast thicknesses up to 60mm. Operation at dose setting L (Low) is not recommended, as the image quality is then below the NHSBSP and European standards.

The dose to the standard breast was 1.48mGy at dose setting H, well below the dose limit of 2.5mGy.

1. Introduction

1.1 Testing procedures and performance standards for digital mammography

This report is one of a series evaluating commercially available direct digital radiography (DR) systems for mammography on behalf of the NHS Breast Screening Programme (NHSBSP). The testing methods and standards applied are mainly derived from NHSBSP Equipment Report 0604[1] which is referred to in this document as 'the NHSBSP protocol'. The standards for image quality and dose are the same as those provided in the European protocol,[2,3] but the latter has been followed where it provides a more detailed standard, for example, for the automatic exposure control (AEC) system.

Some additional tests were carried out according to the UK recommendations for testing mammography X-ray equipment, as described in IPEM Report 89.[4]

1.2 Objectives

The aims of the evaluation were:

- to determine whether the Fujifilm AMULET Innovality digital mammography system meets the main standards in the NHSBSP and European protocols
- to provide performance data for comparison against other systems

2. Method

2.1 System tested

The tests were conducted at the Breast Unit at Barnsley Hospital, on a Fujifilm AMULET Innovality system as described in Table 1. All tests in this report were carried out using the "QC Test" image format (manufacturer's parameters: Max 4.0 mammo, S=121, L=4) The Innovality system is shown in Figure 1.

Table 1. System description

Manufacturer	Fujifilm
Model	AMULET Innovality
Target material	Tungsten
Added filtration	Rhodium
Detector type	Amorphous selenium
Detector serial number	J125020
Image pixel size	50µm
Detector pixel size	Hexagonal pixels with an area equivalent to that of a 68µm square pixel
Detector size	240mm x 300mm
Pixel array	4728 x 5928
Pixel value relationship to dose	Logarithmic
Source to detector distance	650mm
Source to table distance	633mm
Automatic exposure control (AEC) modes	AEC, iAEC
Software version	FDR-3000AWS Mainsoft V5.1

Two AEC modes are available for use with the Innovality: AEC and iAEC.

Both modes can operate at three different dose settings: N (Normal), L (Low) and H (High). Exposures under both AEC modes are determined by a pre-exposure, which does not contribute to the image and is excluded from the mAs shown for the image. The kV and mAs for the pre-exposure are recorded separately in the DICOM header for the image.

iAEC uses all the pixel data from the detector in the pre-exposure to calculate the breast area, breast composition (dense, fatty, implant) and dense area position. The appropriate exposure factors (kV and mAs) are determined from this information.

The AEC mode is similar to the original AMULET's AEC. It uses the pixel values from regions at a fixed distance from the chest wall edge (CWE) to calculate the exposure. The AEC mode was intended for use in quality control (QC) tests, in case there was variation in how the PMMA was set up. However, the iAEC mode used with PMMA was found by the manufacturer to give a stable and consistent result so the AEC mode need not be used for QC.

2.2 Output and HVL

The output and half-value-layer (HVL) were measured as described in the NHSBSP protocol, at intervals of 3kV.

Figure 1. The Fujifilm AMULET Innovality

2.3 Detector response

The detector response was measured as described in the NHSBSP protocol, with a 45mm block of polymethyl-methacrylate (PMMA) at the tube head. An ion chamber was positioned above the table, 40mm from the CWE. The incident air kerma was measured at the detector surface for a range of manually set mAs values at 29kV. The readings were corrected to the surface of the detector using the inverse square law. No correction was made for attenuation by the table and detector cover. Images acquired at the same mAs values were saved as unprocessed files. They were transferred to another computer for analysis. A 10mm square region of interest (ROI) was positioned

on the midline, 40mm from the CWE of each image. The average pixel value and the standard deviation of pixel values within that region were measured. The relationship between average pixel values and the detector entrance surface air kerma was determined.

2.4 Dose measurement

Doses were measured using the X-ray set's AEC in the iAEC mode to expose different thicknesses of PMMA. All three dose settings, N, L and H, were used for these measurements. Each PMMA block had an area of 180mm x 240mm. Spacers were used to adjust the paddle height to be equal to the equivalent breast thickness, as shown in Table 3. The exposure factors were noted and mean glandular doses (MGDs) were calculated for equivalent breast thicknesses.

An aluminium square, 10mm x 10mm and 0.2mm thick, was used with the PMMA during these exposures, so that the images produced could be used for the calculation of the contrast-to-noise ratio (CNR), described in Section 2.5. The aluminium square was placed between two 10mm thick slabs of 180mm x 240mm PMMA, on the midline, with its centre 60mm from the CWE. Additional layers of PMMA were placed on top to vary the total thickness.

2.5 Contrast-to-noise ratio

Unprocessed images acquired during the dose measurement were downloaded and analysed to obtain the CNRs. Thirty six small square ROIs (approximately 2.5mm x 2.5mm) were used to determine the average signal and the standard deviation in the signal within the image of the aluminium square (4 ROIs) and the surrounding background (32 ROIs), as shown in Figure 2. Small ROIs are used to minimise distortions due to the heel effect and other causes of non-uniformity.[5] However, because a flat-field correction is applied, this is less important for DR systems than in computed radiography systems. After correcting the pixel values to achieve a linear relationship between pixel value and dose, the CNR was calculated for each image, as defined in the NHSBSP and European Protocols.

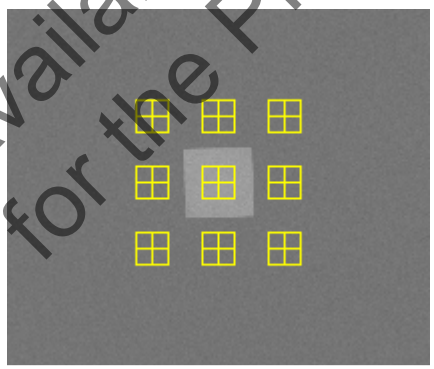

Figure 2. Location and size of ROI used to determine the CNR

To apply the standards in the European protocol, it is necessary to relate the image quality measured using the CDMAM (Section 2.8) for an equivalent breast thickness of 60mm, to that for other breast thicknesses. The European protocol[2] gives the relationship between threshold contrast and CNR measurements, enabling the calculation of a target CNR value for a particular level of image quality. This can be compared to CNR measurements made at other breast thicknesses. Contrast for a particular gold thickness is calculated using Equation 1, and target CNR is calculated using Equation 2.

$$\text{Contrast} = 1 - e^{-\mu t} \quad (1)$$

where μ is the effective attenuation coefficient for gold, and t is the gold thickness.

$$\text{CNR}_{\text{target}} = \frac{\text{CNR}_{\text{measured}} \times \text{TC}_{\text{measured}}}{\text{TC}_{\text{target}}} \quad (2)$$

where $\text{CNR}_{\text{measured}}$ is the CNR for a 60mm equivalent breast, $\text{TC}_{\text{measured}}$ is the threshold contrast calculated using the threshold gold thickness for a 0.1mm diameter detail, (measured using the CDMAM at the same dose as used for $\text{CNR}_{\text{measured}}$), and $\text{TC}_{\text{target}}$ is the calculated threshold contrast corresponding to the threshold gold thickness required to meet either the minimum acceptable or achievable level of image quality as defined in the UK standard.

The 0.1mm detail threshold gold thickness is used here because it is generally regarded as the most critical of the detail diameters for which performance standards are set.

The effective attenuation coefficient for gold used in Equation 1 depends on the beam quality used for the exposure, and was selected from a table of values summarised in Table 2. These values were calculated with 3mm PMMA representing the compression paddle, using spectra from Boone et al.[6] and attenuation coefficients for materials in the test objects (aluminium, gold, PMMA) from Berger et al.[7]

The European protocol also defines a limiting value for CNR, which is calculated as a percentage of the threshold contrast for minimum acceptable image quality for each thickness. This limiting value varies with thickness, as shown in Table 3.

Table 2. Effective attenuation coefficients for gold contrast details in the CDMAM

kV	Target/filter	Effective attenuation coefficient (μm-1)
28	W/Rh	0.134
31	W/Rh	0.122
34	W/Rh	0.109

Table 3. Limiting values for relative CNR

Thickness of PMMA (mm)	Equivalent breast thickness (mm)	Limiting values for relative CNR (%) in European protocol
20	21	> 115
30	32	> 110
40	45	> 105
45	53	> 103
50	60	> 100
60	75	> 95
70	90	> 90

The target CNR values for minimum acceptable and achievable levels of image quality and European limiting values for CNR were calculated. These were compared with the measured CNR results for all breast thicknesses in Section 3.3.2.

2.6 AEC performance for local dense areas

This test is described in the supplement to the fourth edition of the European protocol.[3] To simulate local dense areas, images of a 30mm thick block of PMMA of size 180mm x 240mm, were acquired under AEC, using the iAEC mode. Extra pieces of PMMA between 2 and 20mm thick and of size 20mm x 40mm were added to provide extra attenuation. The compression plate remained in position at a height of 40mm, as shown in Figure 3. The simulated dense area was positioned 50mm from the CWE of the table.

In the simulated local dense area, the mean pixel value and standard deviation for a 10mm x 10mm ROI were measured and the signal-to-noise ratios (SNRs) were calculated. The mean background pixel value in an area adjacent to the dense area was also measured. All pixel values were corrected in order to obtain a linear relationship between pixel value and dose.

Measurements were also made with the greatest thickness (50mm) of total attenuation at alternative positions.

Repeat measurements were carried out using the AEC mode for comparison with the results in the iAEC mode.

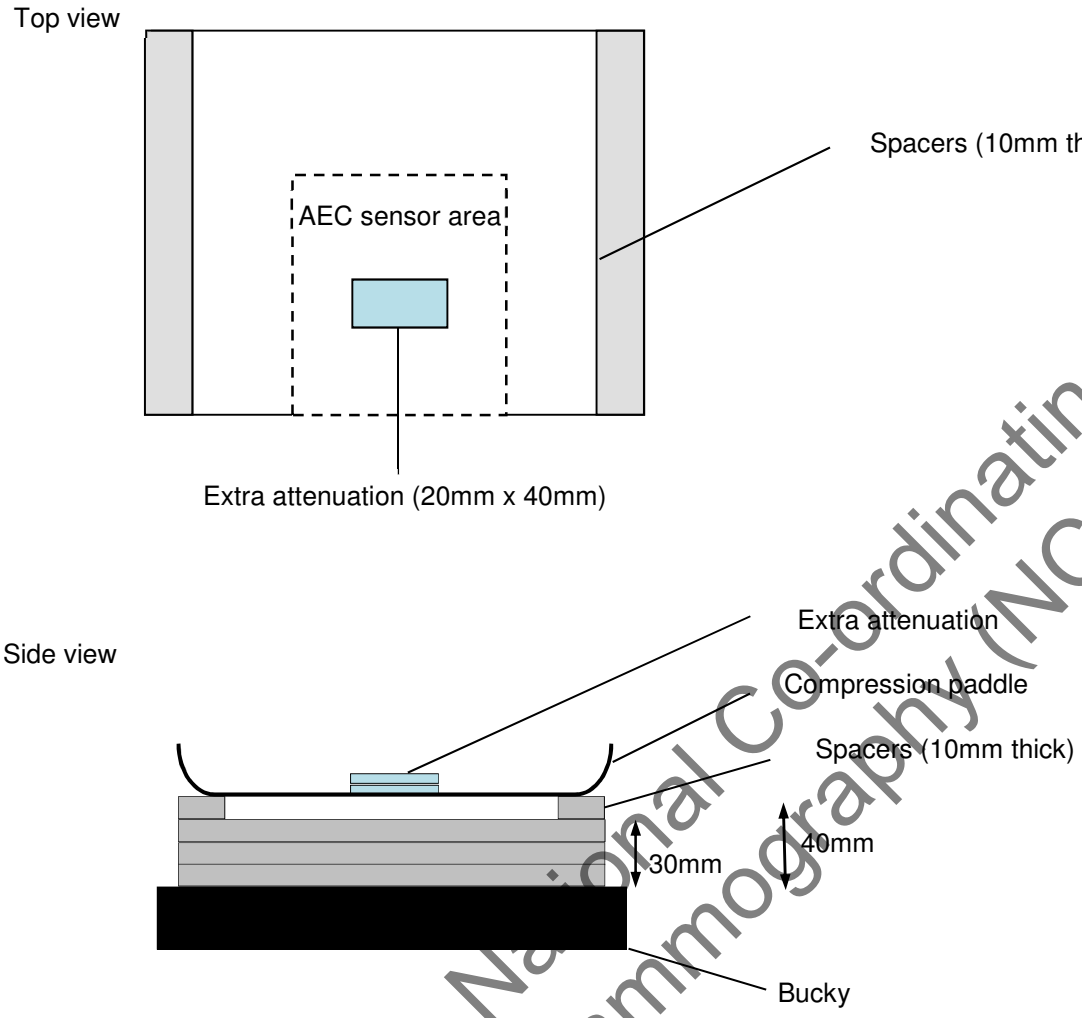

Figure 3. Setup to measure AEC performance for local dense areas

2.7 Noise analysis

The images acquired in the measurements of detector response, using 29kV W/Rh, were used to analyse the image noise. Small ROIs with an area of approximately 2.5mm x 2.5mm were placed on the midline, 60mm from the CWE. The average standard deviations of the pixel values in these ROIs for each image were used to investigate the relationship between the dose to the detector and the image noise. It was assumed that this noise comprises three components: electronic noise, structural noise, and quantum noise. The relationship between them is shown in Equation 3:

$$\sigma_p = \sqrt{k_e^2 + k_q^2 p + k_s^2 p^2} \quad (3)$$

where σ_p is the standard deviation in pixel values within an ROI with a uniform exposure and a mean pixel value p, and k_e, k_q, and k_s are the coefficients determining the amount of electronic, quantum, and structural noise in a pixel with a value p. This method of analysis has been described previously.[8] For simplicity, the noise is generally presented here as relative noise defined as in Equation 4.

$$\text{Relative noise} = \frac{\sigma_p}{p} \quad (4)$$

The variation in relative noise with mean pixel value was evaluated and fitted using Equation 3, and non-linear regression used to determine the best fit for the constants and their asymptotic confidence limits (using Graphpad Prism version 6.05 for Windows, Graphpad software, San Diego, California, USA, www.graphpad.com). This established whether the experimental measurements of the noise fitted this equation, and the relative proportions of the different noise components. The relationship between noise and pixel values has been found empirically to be approximated by a simple power relationship as shown in Equation 5.

$$\frac{\sigma_p}{p} = k_t p^{-n} \quad (5)$$

where k_t is a constant. If the noise were purely quantum noise the value of n would be 0.5. However the presence of electronic and structural noise means that n can be slightly higher or lower than 0.5.

The variance in pixel values within a ROI is defined as the standard deviation squared. The total variance was plotted against incident air kerma at the detector and fitted using Equation 3. Non-linear regression was used to determine the best fit for the constants and their asymptotic confidence limits, using the Graphpad Prism software.

Using the calculated constants, the structural, electronic, and quantum components of the variance were estimated, assuming that each component was independently related to incident air kerma. The percentage of the total variance represented by each component was then calculated and plotted against incident air kerma at the detector.

2.8 Image quality measurements

Contrast detail measurements were made using a CDMAM phantom (serial number 1022, version 3.4, UMC St. Radboud, Nijmegen University, Netherlands). The phantom was positioned with a 20mm thickness of PMMA above and below, to give a total attenuation approximately equivalent to 50mm of PMMA or 60mm thickness of typical breast tissue. The kV and mAs were chosen to match as closely as possible those selected by the AEC, using iAEC mode at dose setting N, when imaging a 50mm thickness of PMMA. This procedure was repeated to obtain a representative sample of 16 images at this dose level. The unprocessed images were transferred to disk for subsequent analysis off-site. Further sets of 16 images of the test phantom were then obtained at other dose levels by manually selecting higher and lower mAs values with the same beam quality.

An automatic method of reading the CDMAM images was used.[9,10] Version 1.6 of CDCOM was used in the analysis. The threshold gold thickness for a typical human observer was predicted using Equation 6.

$$TC_{predicted} = rTC_{auto} \quad (6)$$

where $TC_{predicted}$ is the predicted threshold contrast for a typical observer, TC_{auto} is the threshold contrast measured using an automated procedure with CDMAM images. r is the average ratio between human and automatic threshold contrast determined experimentally with the values shown in Table 4.

The contrasts used in Equation 6 were calculated from gold thickness using the effective attenuation coefficients shown in Table 2.

Table 4. Values of r used to predict threshold contrast

Diameter of gold disc (mm)	Average ratio of human to automatically measured threshold contrast (r)
0.08	1.40
0.10	1.50
0.13	1.60
0.16	1.68
0.20	1.75
0.25	1.82
0.31	1.88
0.40	1.94
0.50	1.98
0.63	2.01
0.80	2.06
1.00	2.11

The predicted threshold gold thickness for each detail diameter in the range 0.1mm to 1.0mm was fitted with a curve for each dose level, using the relationship shown in Equation 7.

$$\text{Threshold gold thickness} = a + bx^{-1} + cx^{-2} + dx^{-3} \quad (7)$$

where x is the detail diameter, and a, b, c and d are coefficients adjusted to obtain a least squares fit.

The confidence limits for the predicted threshold gold thicknesses have been previously determined by a sampling method using a large set of images. The threshold contrasts quoted in the tables of results are derived from the fitted curves, as this has been found to improve accuracy.

The expected relationship between threshold contrast and dose is shown in Equation 8.

$$\text{Threshold contrast} = \lambda D^{-n} \quad (8)$$

where D is the MGD for a 60mm thick standard breast (equivalent to the test phantom configuration used for the image quality measurement), and λ is a constant to be fitted.

It is assumed that a similar equation applies when using threshold gold thickness instead of contrast. This equation was plotted with the experimental data for detail diameters of 0.1 and 0.25mm. The value of n resulting in the best fit to the experimental data was determined, and the doses required for target CNR values were calculated for data relating to these detail diameters.

2.9 Physical measurements of the detector performance

The modulation transfer function (MTF), normalised noise power spectrum (NNPS) and the detective quantum efficiency (DQE) of the system were measured. The methods used were as close as possible to those described by the International Electrotechnical Commission (IEC).[11] The radiation quality used for the measurements was adjusted by placing a uniform 2mm thick aluminium filter at the tube housing. The beam quality used was 29kV W/Rh. The test device to measure the MTF comprised of a 120mm x 60mm rectangle of stainless steel with polished straight edges, of thickness 0.8mm. This test device was placed directly on the breast support table, and the grid was removed by selecting “grid out” at the operator console. The test device was positioned to measure the MTF in two directions, first almost perpendicular to the CWE and then almost parallel to it.

To measure the noise power spectrum the test device was removed and exposures made for a range of incident air kerma at the surface of the table. The DQE is presented as the average of measurements in the directions perpendicular and parallel to the CWE.

2.10 Optimisation

A method for determining optimal beam qualities and exposure factors for digital mammography systems has been described previously and was used to evaluate this system.[8,12] CNR and MGD were measured as described above, using blocks of PMMA, 20 to 70mm thick. For each thickness, a range of voltage settings were used and the post-exposure mAs values were recorded. The MGDs to typical breasts equivalent to each thickness of the PMMA were calculated, as described in the NHSBSP protocol. Exposures were made under AEC in iAEC mode. The relationship between noise and pixel values in digital mammography systems has been previously[8] shown to be approximated by:

$$\text{Relative noise} = \frac{\sqrt{\frac{sd(bgd)^2 + sd(Al)^2}{2}}}{p} = k_t p^{-n} \quad (9)$$

where k_t is a constant, p is the average background pixel value linearised with absorbed dose to the detector, $sd(bgd)$ is the average standard deviation of pixel values in the ROIs over the background, and $sd(Al)$ is the average standard deviation of pixel values in an ROI over a piece of aluminium of size 10mm x 10mm and 0.2mm thick. The value of n was found by fitting this equation to the experimental data. Equation 10 was then used to calculate the dose required to achieve a target CNR, where k is a constant to be fitted, and D is the MGD for a breast of equivalent thickness.

$$CNR = kD^n \quad (10)$$

Target CNRs were calculated to reach the minimum and achievable levels of image quality as specified in the NHSBSP and European protocols using the following relationship:

$$\text{Threshold contrast} = \frac{\lambda}{CNR} \quad (11)$$

where λ is a constant that is independent of dose, beam quality and the thickness of attenuating material.

The optimal beam quality for each thickness was selected as that necessary to achieve the target CNR for the minimum dose.

2.11 Other tests

Other tests were carried out to cover the range that would normally form part of a commissioning survey on new equipment. These included tests prescribed in IPEM Report 89[4] for mammographic X-ray sets, as well as those in the UK NHSBSP protocol for digital mammographic systems. The tests measured tube voltage, accuracy of indicated compressed breast thickness, compression force, alignment of radiation field to light field and image, image retention, focal spot dimensions, AEC reproducibility, image uniformity, cycle time and backup timer.

3. Results

3.1 Output and HVL

The output and HVL measurements are shown in Table 5.

Table 5. Output and HVL

kV	Target/filter	Output (μGy/mAs at 1m)	HVL (mm Al)
25	W/Rh	10.0	0.49
28	W/Rh	14.2	0.53
31	W/Rh	18.1	0.56
34	W/Rh	22.0	0.58

3.2 Detector response

The detector response is shown in Figure 4.

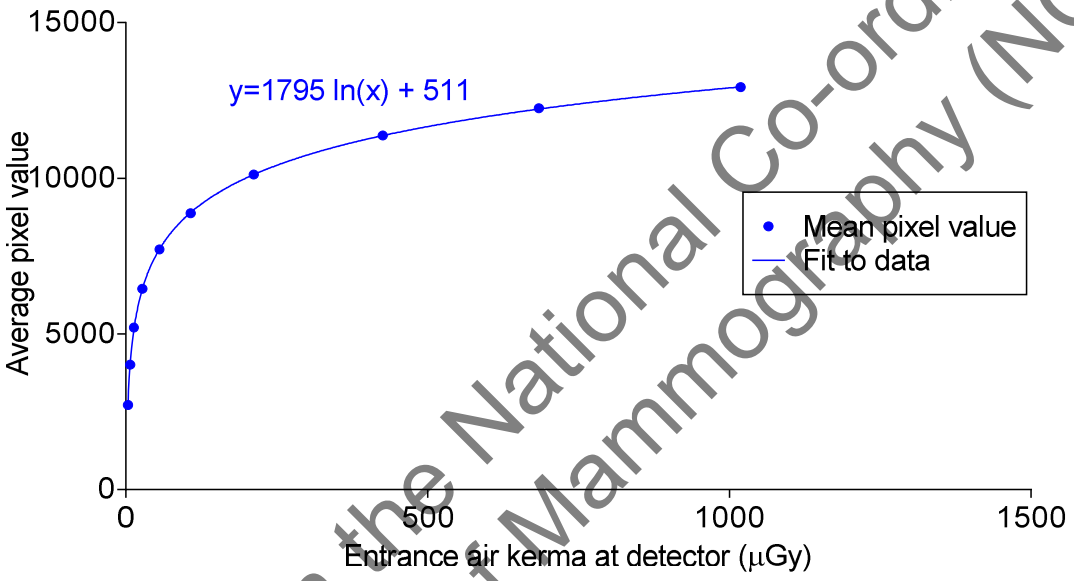

Figure 4. Detector response

3.3 AEC performance

3.3.1 Dose

The MGDs for breasts simulated with PMMA, exposed under AEC using the iAEC mode, are shown in Table 6 and Figure 5. The mAs values exclude the pre-exposure. The MGDs are calculated from the total mAs, including the pre-exposure.

Table 6. MGD for simulated breasts, using iAEC

PMMA thickness (mm)	Equivalent breast thickness (mm)	kV	Target/ filter	Dose setting N		Dose setting L		Dose setting H	
				mAs	MGD (mGy)	mAs	MGD (mGy)	mAs	MGD (mGy)
20	21	26	W/Rh	32.4	0.52	18.2	0.30	47.6	0.75
30	32	27	W/Rh	47.3	0.69	27.6	0.42	69.1	1.00
40	45	28	W/Rh	64.8	0.90	36.5	0.53	94.2	1.29
45	53	29	W/Rh	70.5	1.03	40.2	0.61	103.6	1.48
50	60	30	W/Rh	79.2	1.19	45.8	0.72	116.7	1.73
60	75	31	W/Rh	109.0	1.57	62.5	0.95	161.2	2.28
70	90	33	W/Rh	141.0	2.06	80.9	1.23	207.3	2.97

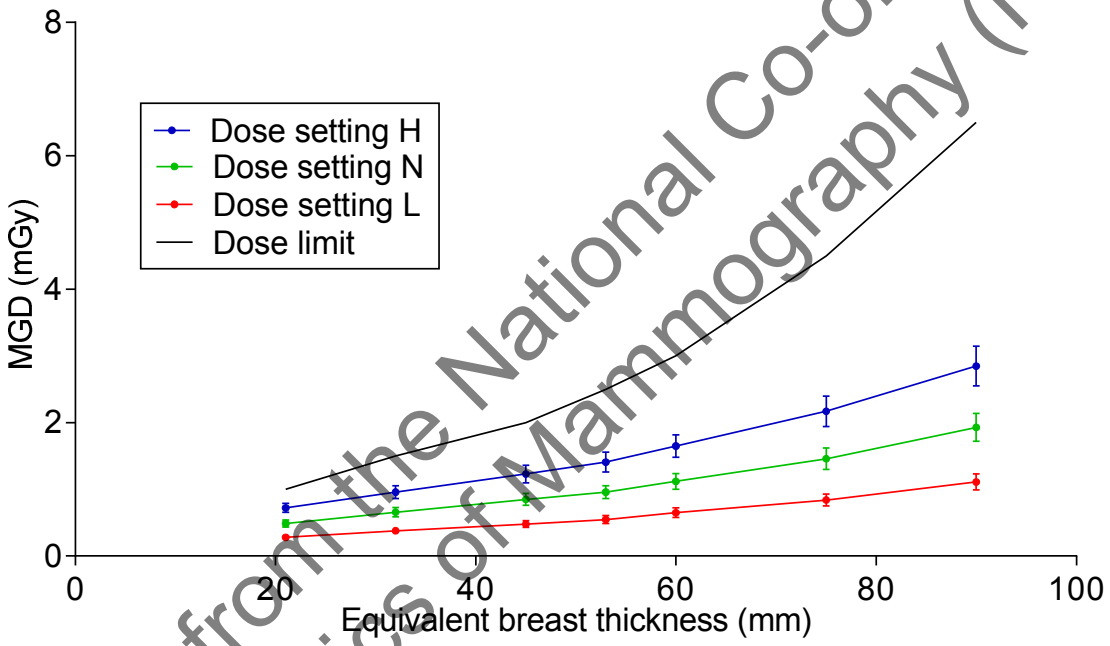

Figure 5. MGD for different thicknesses of simulated breasts at the three dose settings using iAEC. (Error bars indicate 95% confidence limits.)

3.3.2 CNR

The results of the CNR measurements are shown in Table 7 and Figure 6. The following calculated values are also shown:

- CNR to meet the minimum acceptable image quality standard at the 60mm breast thickness
- CNR to meet the achievable image quality standard at the 60mm breast thickness
- CNRs at each thickness to meet the limiting value in the European protocol

Table 7. CNR measurements

PMMA (mm)	Equivalent breast thickness (mm)	Measured CNR (Dose setting N)	Measured CNR (Dose setting L)	Measured CNR (Dose setting H)	CNR for minimum acceptable IQ	CNR for achievable IQ	European limiting CNR value
20	21	8.7	6.5	10.6	3.8	5.7	4.4
30	32	7.6	5.8	9.5	3.8	5.7	4.2
40	45	6.7	5.0	8.0	3.8	5.7	4.0
45	53	6.1	4.5	7.6	3.8	5.7	3.9
50	60	5.7	4.3	7.0	3.8	5.7	3.8
60	75	5.0	3.7	6.1	3.8	5.7	3.6
70	90	4.4	3.1	5.2	3.8	5.7	3.5

Table 8 shows the mean pixel values measured in the background region for the CNR measurements, corrected to obtain a linear relationship between pixel value and dose.

Table 8. Mean corrected (linearised) background pixel values measured under iAEC

PMMA (mm)	Equivalent breast thickness (mm)	Pixel value (Dose setting N)	Pixel value (Dose setting L)	Pixel value (Dose setting H)
20	21	98	56	144
30	32	91	53	132
40	45	79	46	115
45	53	75	44	111
50	60	75	44	111
60	75	70	41	106
70	90	82	47	121

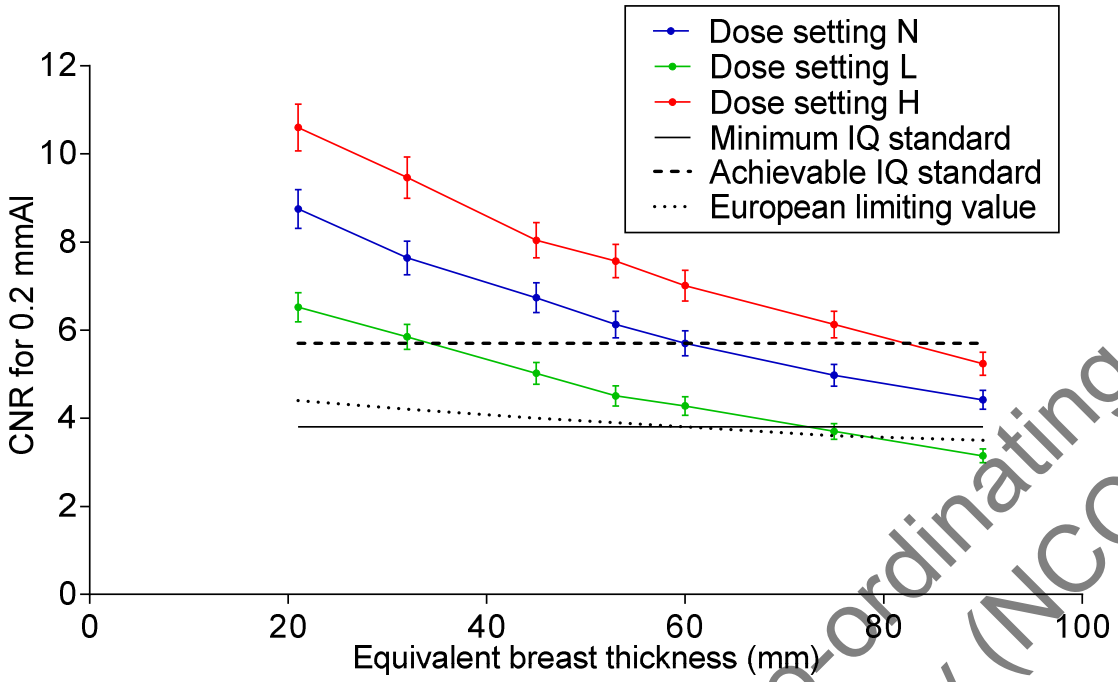

Figure 6. CNR measured using iAEC at the three dose settings. (Error bars indicate 95% confidence limits.)

3.3.3 AEC performance for local dense areas

It is expected that when the AEC adjusts for locally dense areas, the SNR will remain constant with increasing thickness of extra PMMA. The results, obtained with the AEC in iAEC mode, are presented in Table 9 and Figure 7. They show that the SNR varied by no more than 3% from the mean value while the local dense area was positioned on the midline, 50mm from the CWE of the breast support table. Moving the dense area 50mm laterally and closer to the CWE also produced the same SNR within the dense area. The kV decreased and SNR dropped when the dense area was positioned 80mm from the CWE, suggesting that the dense area in this position was not detected. The increasing dose selected in iAEC mode to achieve this constant SNR within the increasingly dense area is indicated by the linearised background pixel value which is also shown in Table 9 and Figure 7.

For comparison the results obtained using the AEC mode are shown in Table 10 and Figure 8.

Table 9. AEC performance (in iAEC mode) for local dense areas

Total attenuation (mm PMMA)	Position of local dense area: From midline of table (mm)	Position of local dense area: From CWE (mm)	kV	Target/ filter	Tube load (mAs)	Linearised background pixel value	SNR	% SNR difference from first SNR result
32	0	50	28	W/Rh	44.1	94	47.6	–
34	0	50	28	W/Rh	49.0	104	48.3	1
36	0	50	28	W/Rh	54.6	114	47.7	0
38	0	50	29	W/Rh	54.2	130	47.8	0
40	0	50	29	W/Rh	64.7	153	49.1	3
42	0	50	29	W/Rh	71.6	171	49.5	4
44	0	50	30	W/Rh	71.3	195	50.2	5
46	0	50	30	W/Rh	78.8	214	49.5	4
48	0	50	30	W/Rh	87.0	235	49.2	3
50	0	50	30	W/Rh	96.5	260	48.6	2
50	0	80	28	W/Rh	37.0	78	24.7	-48
50	0	30	30	W/Rh	99.9	268	49.7	4
50	50	30	30	W/Rh	99.9	268	48.6	2
50	50	60	30	W/Rh	100.0	268	48.3	1
50	50	80	28	W/Rh	37.0	77	24.2	-49
50	0	60	30	W/Rh	96.5	259	48.6	2

Table 10. AEC performance (in AEC mode) for local dense areas

Total attenuation (mm PMMA)	kV target	Target/ filter	Tube load (mAs)	Linearised background pixel value	SNR	% difference from first SNR result
32	28	W/Rh	38.6	87.6	44.7	–
34	28	W/Rh	38.5	87.6	44.6	0
36	28	W/Rh	38.8	88.1	42.3	-5
38	28	W/Rh	38.9	88.4	40.2	-10
40	28	W/Rh	38.6	87.6	37.1	-17
42	28	W/Rh	52.3	117.6	40.9	-8
44	28	W/Rh	56.9	129.9	41.4	-7
46	28	W/Rh	58.0	130.0	36.3	-19
48	28	W/Rh	61.4	134.8	34.8	-22
50	29	W/Rh	73.0	186.4	39.4	-12

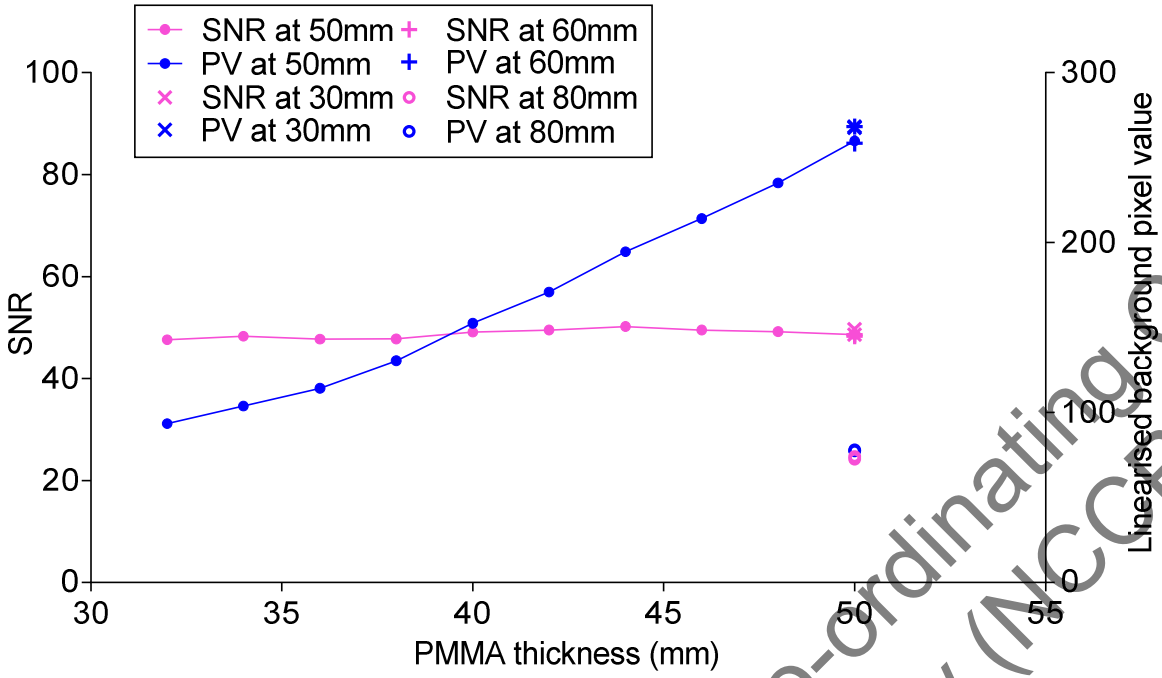

Figure 7. AEC performance (in iAEC mode) for local dense areas with measurements made at different distances from the CWE

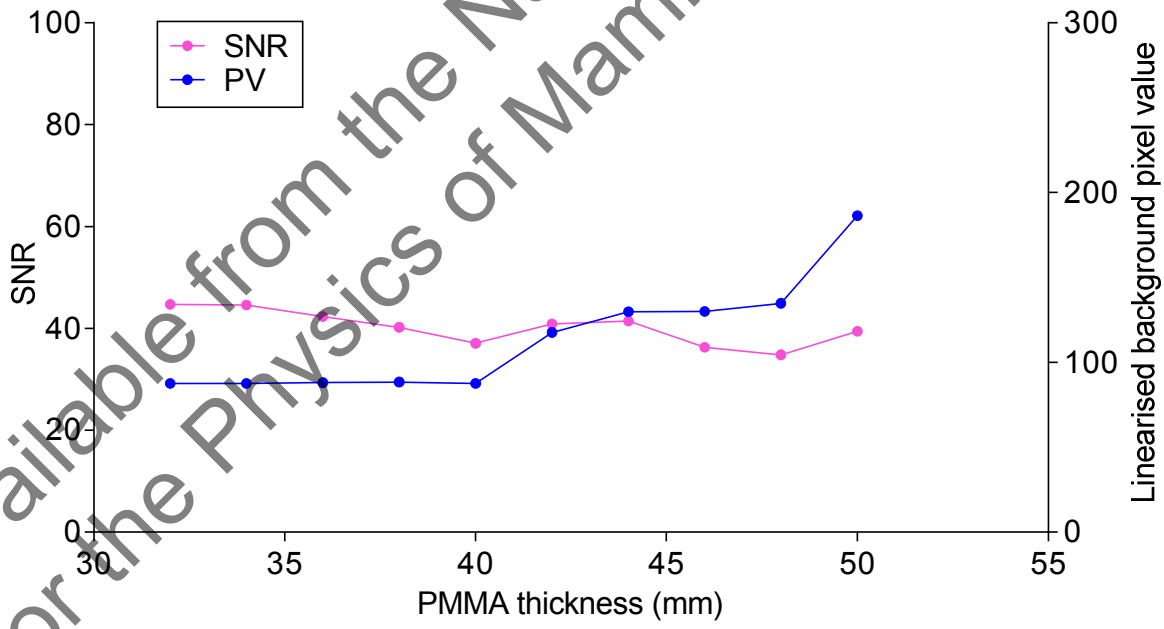

Figure 8. AEC performance (in AEC mode) for a local dense area at a distance of 50mm from the CWE

3.4 Noise measurements

The variation in noise with dose was analysed by plotting the standard deviation in pixel values against the detector entrance air kerma, as shown in Figure 9. The fitted power curve has an index of 0.50, which is the expected value for quantum noise sources alone.

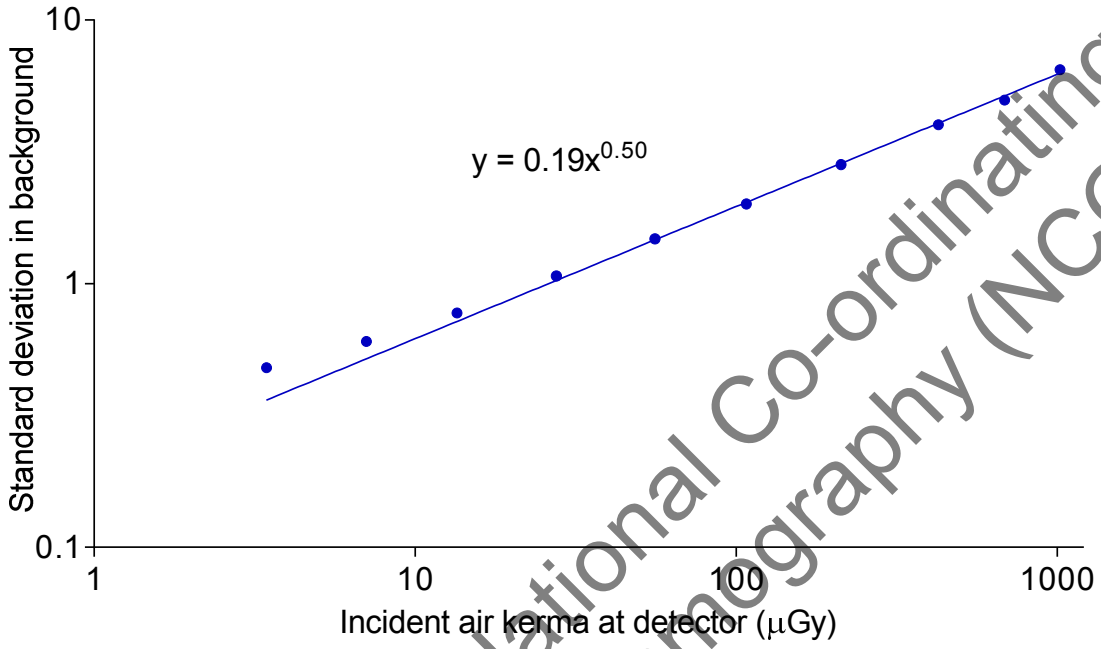

Figure 9. Standard deviation of linearized pixel values versus air kerma at detector

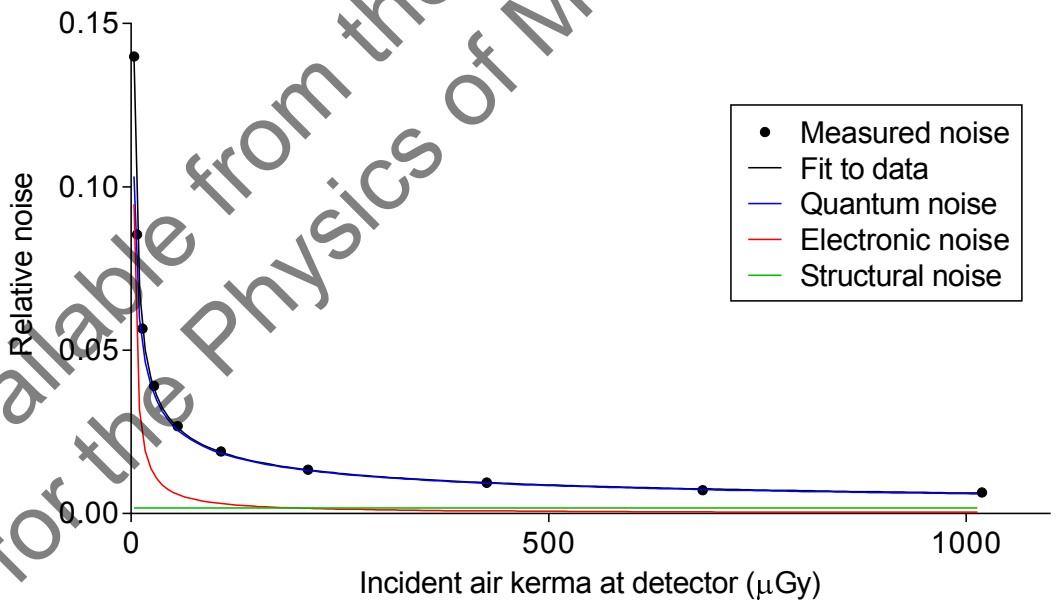

Figure 10. Relative noise and noise components

Figure 10 is an alternative way of presenting the data and shows the relative noise at different entrance air kerma. The estimated relative contributions of electronic,

structural, and quantum noise are shown and the quadratic sum of these contributions fitted to the measured noise (using Equation 3). From this, the dose range over which the quantum component dominates can be seen.

Figure 11 shows the different amounts of variance due to each component, and the percentage quantum variance is seen in comparison to the 80% limit. Dotted lines indicate the AEC operating level.

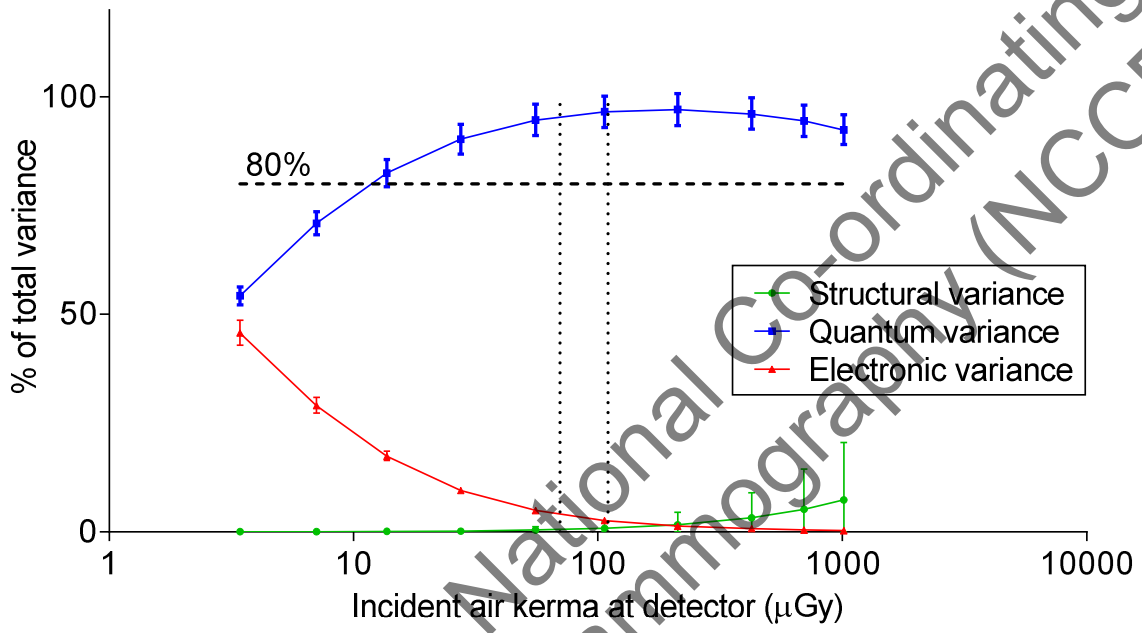

Figure 11. Noise components as a percentage of the total variance. (Error bars indicate 95% confidence limits.)

3.5 Image quality measurements

The exposure factors used for each set of 16 CDMAM images are shown in Table 11. The MGDs ranged from half to double the dose of 1.12mGy, which was selected using iAEC at dose setting N.

Table 11. Images acquired for image quality measurement

kV	Target/filter	Tube loading (mAs)	Mean glandular dose to equivalent breasts 60mm thick (mGy)
30	W/Rh	40	0.57
30	W/Rh	63	0.89
30	W/Rh	79	1.12
30	W/Rh	124	1.76
30	W/Rh	158	2.24

The contrast detail curves (determined by automatic reading of the images) at the different dose levels are shown in Figure 12. The threshold gold thicknesses measured for different detail diameters at the 5 selected dose levels are shown in Table 12. The NHSBSP minimum acceptable and achievable limits are also shown.

The measured threshold gold thicknesses are plotted against the MGD for an equivalent breast for the 0.1mm and 0.25mm detail sizes in Figure 13.

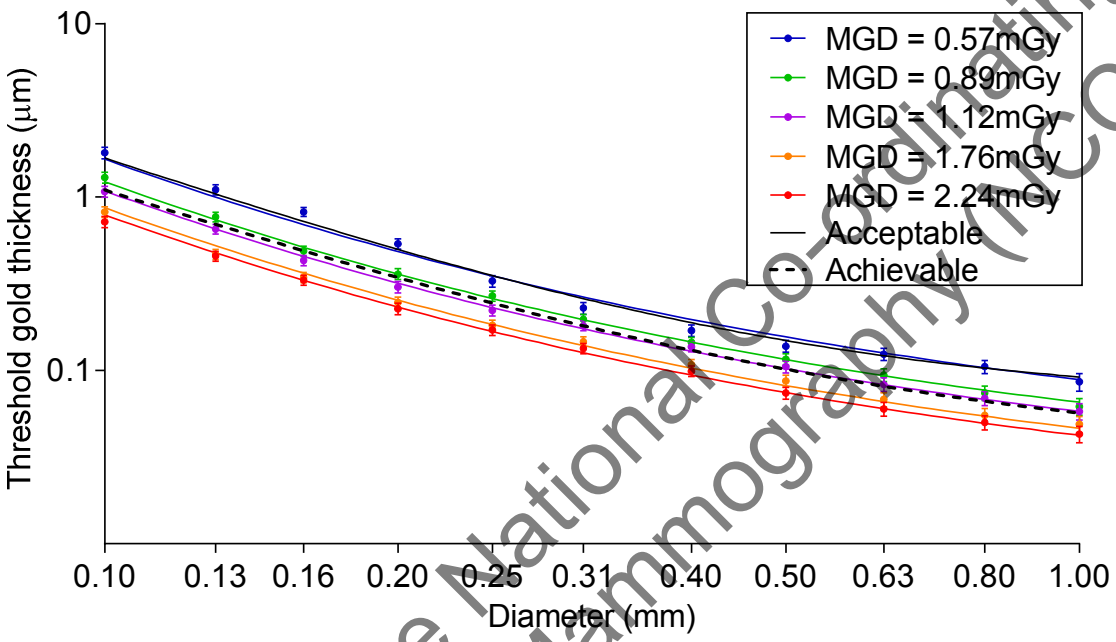

Figure 12. Contrast-detail curves for 5 doses at 30kV W/Rh. (Error bars indicate 95% confidence limits.)

Table 12. Average threshold gold thicknesses for different detail diameters for 5 doses using 30kV W/Rh, and automatically predicted data

Diam-eter (mm)	Threshold gold thickness (µm)						
	Accept-able value	Achiev-able value	MGD = 0.57mGy	MGD = 0.89mGy	MGD = 1.12mGy	MGD = 1.76mGy	MGD = 2.24mGy
0.1	1.680	1.100	1.800 ± 0.139	1.296 ± 0.095	1.077 ± 0.079	0.821 ± 0.059	0.719 ± 0.053
0.25	0.352	0.244	0.328 ± 0.025	0.269 ± 0.019	0.222 ± 0.016	0.182 ± 0.013	0.171 ± 0.012
0.5	0.150	0.103	0.138 ± 0.011	0.116 ± 0.009	0.105 ± 0.008	0.087 ± 0.007	0.074 ± 0.006
1	0.091	0.056	0.086 ± 0.010	0.062 ± 0.007	0.058 ± 0.006	0.049 ± 0.005	0.043 ± 0.005

3.6 Comparison with other systems

The MGDs to reach the minimum and achievable image quality standards in the NHSBSP protocol have been estimated from the curves shown in Figure 13. The fitted

curves are of the form $y = x^{-n}$. (The error in estimating these doses depends on the accuracy of the curve fitting procedure, and pooled data for several systems has been used to estimate the 95% confidence limits of about 20%.) These doses are shown against similar data for different models of digital mammography systems in Tables 13 and 14 and Figures 14 to 17. The data for these systems has been determined in the same way as described in this report and the results published previously.[13-20] The data for film-screen represents an average value determined using a variety of film-screen systems in recent use.

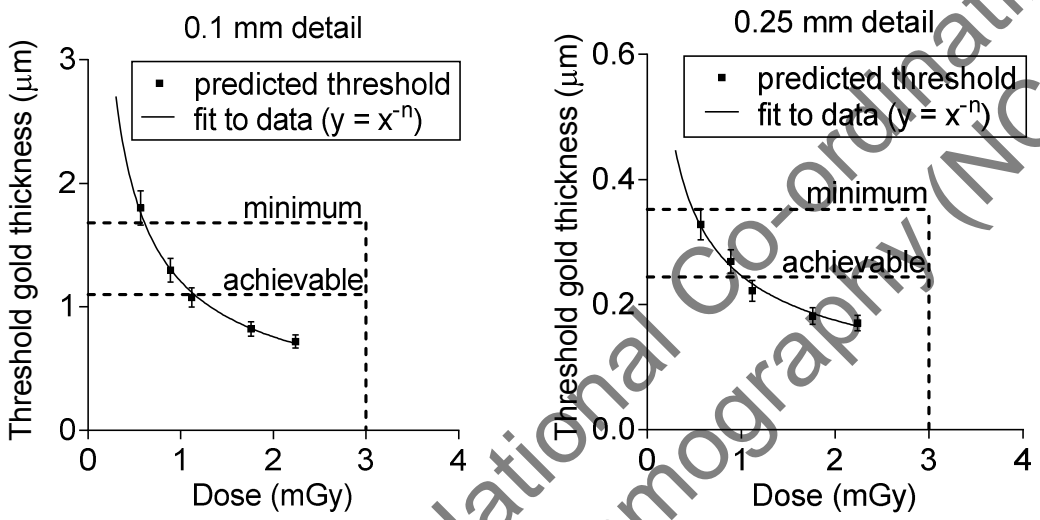

Figure 13. Threshold gold thickness at different doses. (Error bars indicate 95% confidence limits.)

Table 13. The MGD for a 60mm equivalent breast for different systems to reach the minimum threshold gold thickness for 0.1mm and 0.25mm details

System	MGD (mGy) for 0.1mm	MGD (mGy) for 0.25mm
Fujifilm AMULET f/s	0.79 ± 0.16	0.58 ± 0.12
Fujifilm Innovality	**0.61 ± 0.12**	**0.49 ± 0.10**
GE Essential	0.49 ± 0.10	0.49 ± 0.10
Hologic Dimensions (v1.4.2)	0.34 ± 0.07	0.48 ± 0.10
Hologic Selenia (W)	0.71 ± 0.14	0.64 ± 0.13
IMS Giotto 3DL	0.93 ± 0.19	0.70 ± 0.14
Philips MicroDose L30 C120	0.67 ± 0.13	0.47 ± 0.09
Siemens Inspiration	0.76 ± 0.15	0.60 ± 0.12
Film-screen	1.30 ± 0.26	1.36 ± 0.27
Agfa CR85-X (NIP)	1.27 ± 0.25	0.96 ± 0.19
Fujifilm Profect CR	1.78 ± 0.36	1.35 ± 0.27

Table 14. The MGD for a 60mm equivalent breast for different systems to reach the achievable threshold gold thickness for 0.1mm and 0.25mm details

System	MGD (mGy) for 0.1mm	MGD (mGy) for 0.25mm
Fujifilm AMULET f/s	1.35 ± 0.27	1.58 ± 0.32
Fujifilm Innovality	**1.15 ± 0.23**	**1.02 ± 0.20**
GE Essential	1.13 ± 0.13	1.03 ± 0.21
Hologic Dimensions (v1.4.2)	0.87 ± 0.17	1.10 ± 0.22
Hologic Selenia (W)	1.37 ± 0.27	1.48 ± 0.30
IMS Giotto 3DL	1.60 ± 0.32	1.41 ± 0.28
Philips MicroDose L30 C120	1.34 ± 0.27	1.06 ± 0.21
Siemens Inspiration	1.27 ± 0.25	1.16 ± 0.23
Film-screen	3.03 ± 0.61	2.83 ± 0.57
Agfa CR (NIP)	2.47 ± 0.49	2.34 ± 0.47
Fujifilm Profect CR	3.29 ± 0.66	2.65 ± 0.53

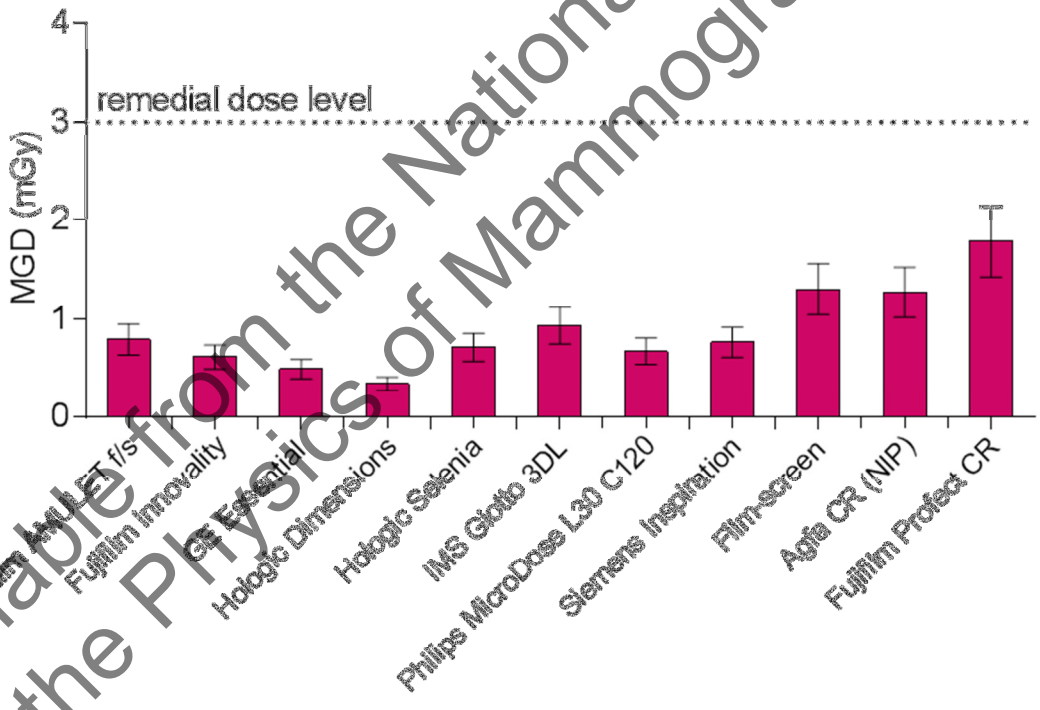

Figure 14. MGD for a 60mm equivalent breast to reach minimum acceptable image quality standard for 0.1mm detail. (Error bars indicate 95% confidence limits.)

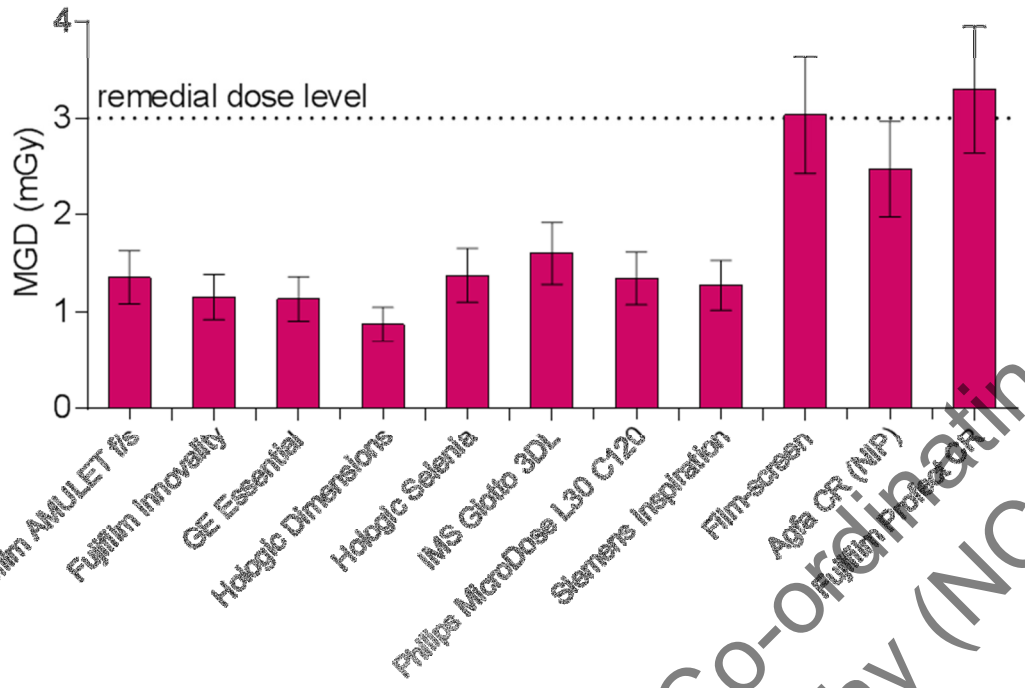

Figure 15. MGD for a 60mm equivalent breast to reach achievable image quality standard for 0.1mm detail. (Error bars indicate 95% confidence limits.)

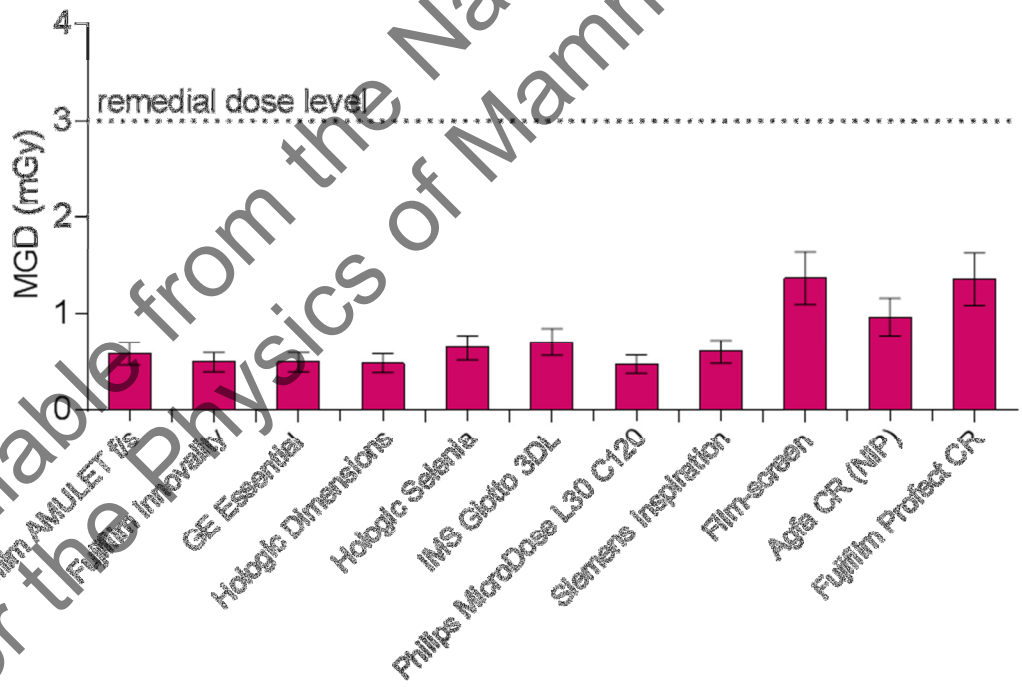

Figure 16. MGD for a 60mm equivalent breast to reach minimum acceptable image quality standard for 0.25mm detail. (Error bars indicate 95% confidence limits.)

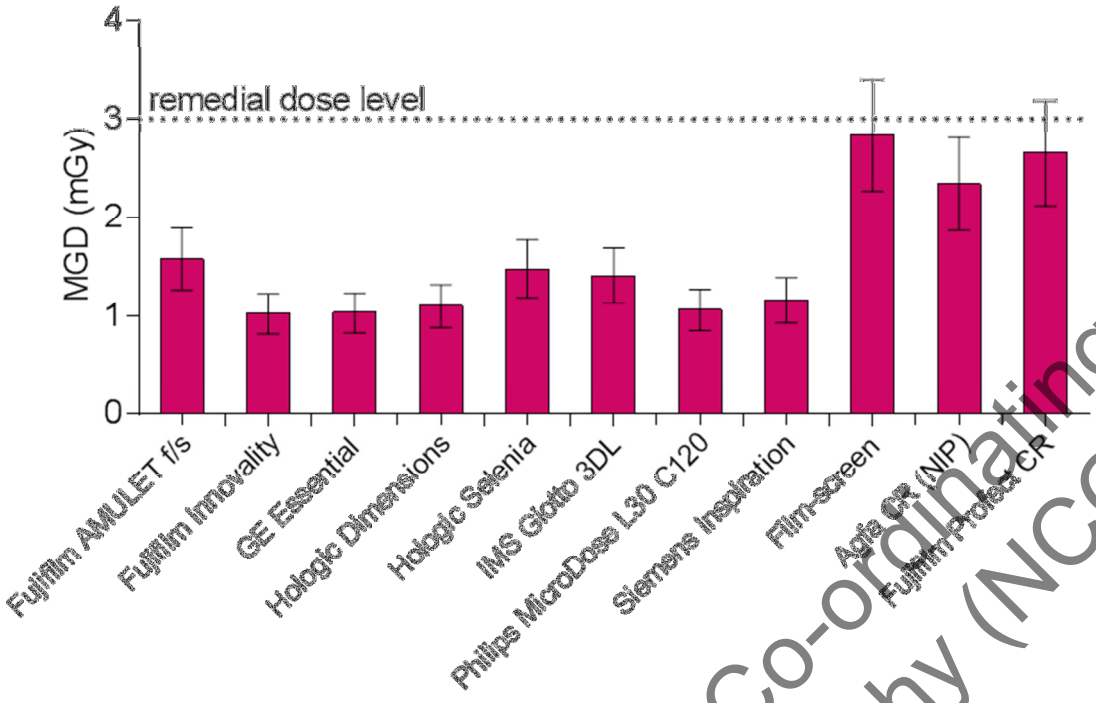

Figure 17. MGD for a 60mm equivalent breast to reach achievable image quality standard for 0.25mm detail. (Error bars indicate 95% confidence limits.)

3.7 Detector performance

The MTF is shown in Figure 18 for the two orthogonal directions. Figure 19 shows the NNPS curves for a range of entrance air kerma.

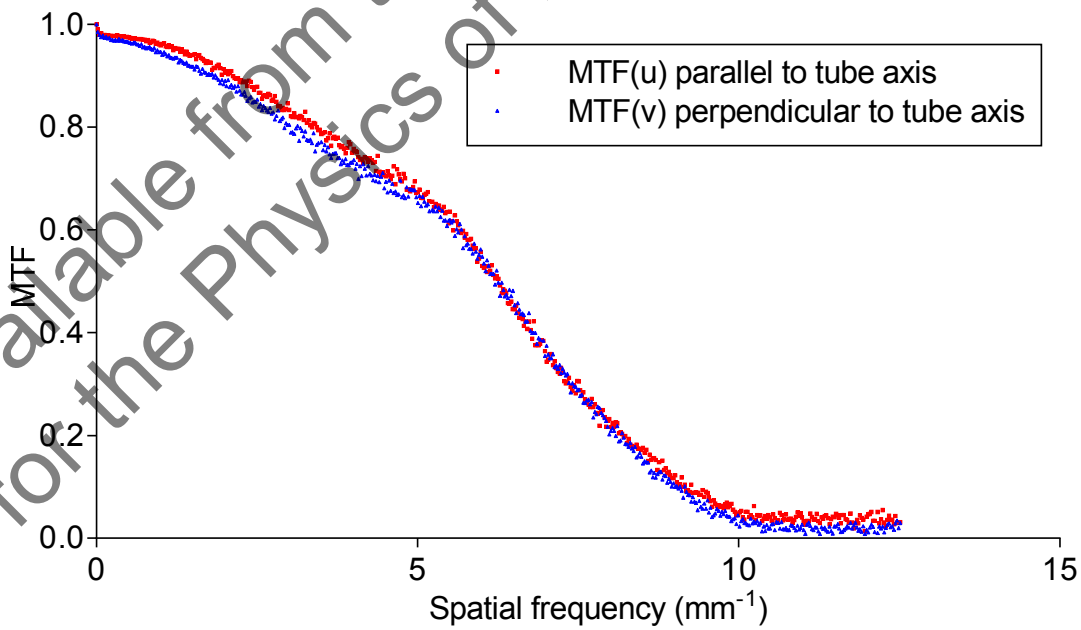

Figure 18. Pre-sampling MTF

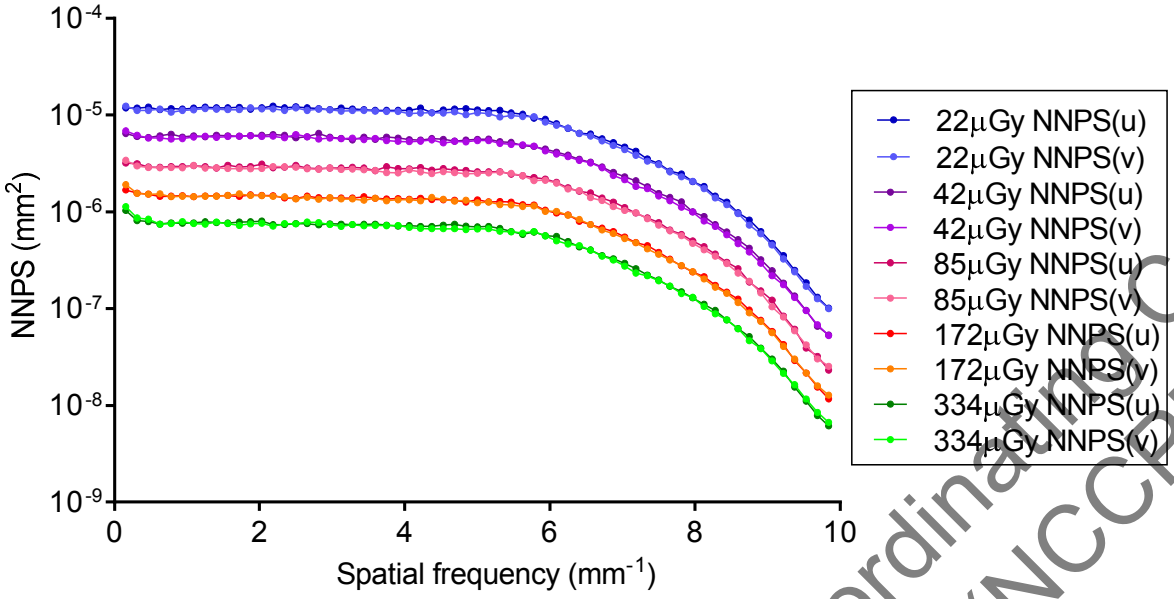

Figure 19. NNPS curves for a range of entrance air kerma

Figure 20 shows the DQE averaged in the two orthogonal directions for a range of entrance air kerma. The MTF and DQE measurements were interpolated to show values at standard frequencies in Table 15.

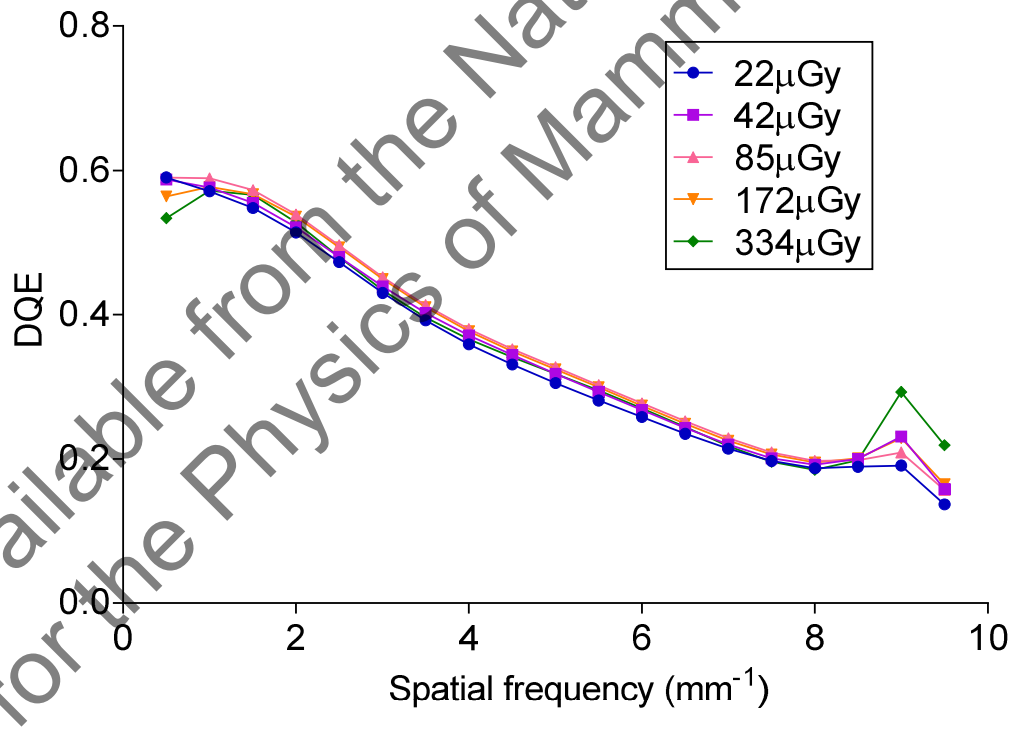

Figure 20. DQE averaged in both directions for a range of entrance air kerma

Table 15. MTF and DQE measurements at standard frequencies (DQE at 85µGy)

Frequency (mm^{-1})	MTF (u)	MTF (v)	MTF (uv)	DQE (uv)
0.0	0.98	0.98	0.98	0.60
0.5	0.98	0.96	0.97	0.59
1.0	0.96	0.95	0.96	0.59
1.5	0.94	0.92	0.93	0.57
2.0	0.90	0.88	0.89	0.54
2.5	0.87	0.84	0.85	0.50
3.0	0.83	0.80	0.82	0.45
3.5	0.80	0.77	0.78	0.41
4.0	0.76	0.73	0.75	0.38
4.5	0.72	0.70	0.71	0.35
5.0	0.67	0.65	0.66	0.33
5.5	0.61	0.60	0.60	0.30
6.0	0.54	0.53	0.53	0.28
6.5	0.46	0.46	0.46	0.25
7.0	0.38	0.38	0.38	0.23
7.5	0.30	0.30	0.30	0.21
8.0	0.22	0.22	0.22	0.20
8.5	0.16	0.15	0.16	0.20
9.0	0.11	0.10	0.10	0.21
9.5	0.08	0.06	0.07	0.16

3.8 Optimisation

The target CNR corresponding to the achievable image quality was calculated to be 5.7. The MGD required to reach this target CNR for a range of beam qualities and different thicknesses of PMMA is shown in Figure 21.

Table 16 shows the optimal beam qualities selected from this data with corresponding mAs values. The table also shows the MGDs calculated with the optimal exposure factors, and with the factors selected by iAEC at dose setting N (excluding pre-exposure).

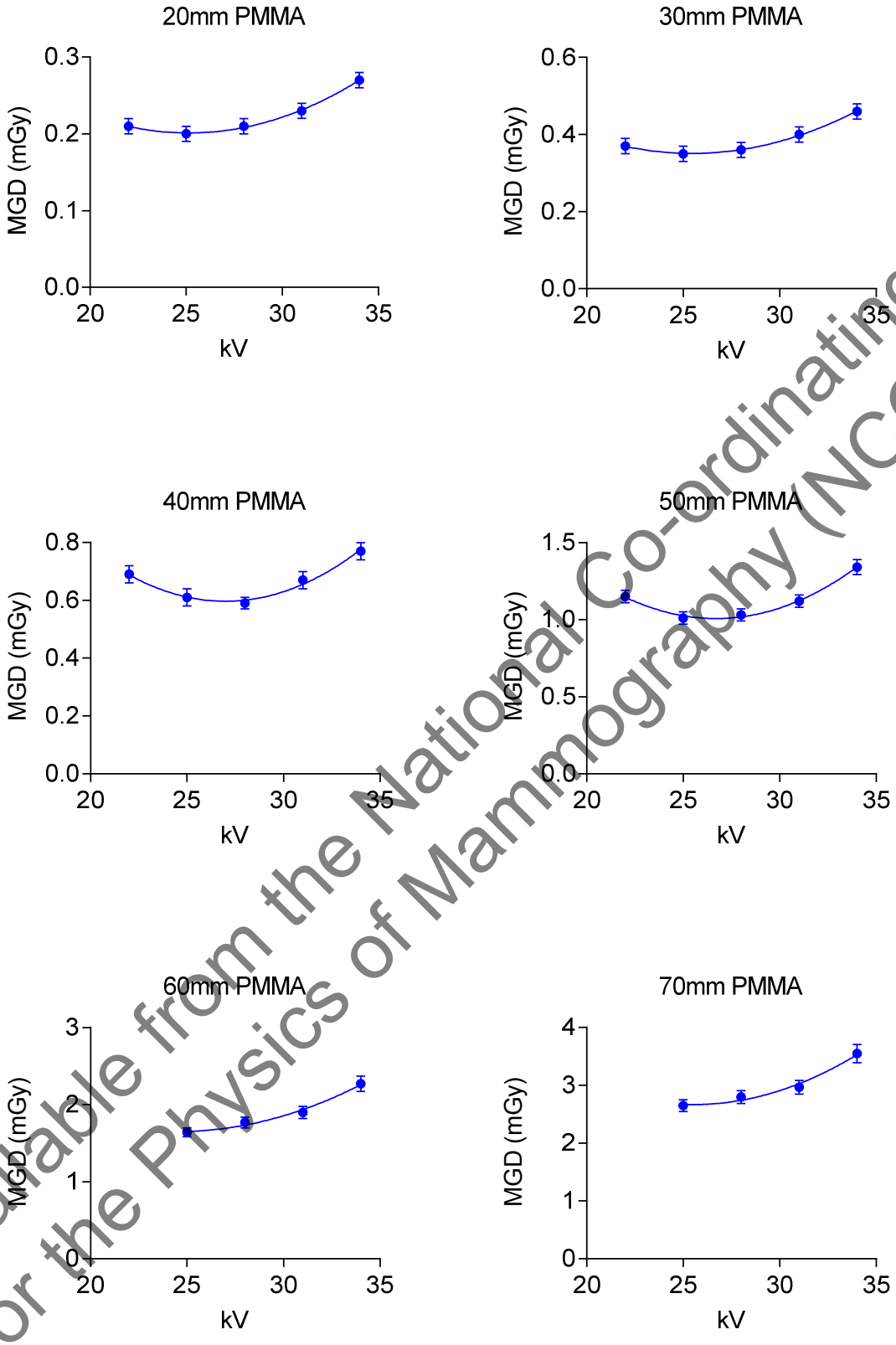

Figure 21. MGD to reach the achievable image quality standard in the NHSBSP protocol. (Error bars indicate 95% confidence limits.)

Table 16. Optimal factors for achievable image quality (where CNR = 5.7)

PMMA thickness (mm)	kV	Target/ filter	mAs	MGD (mGy) with optimal factors	MGD (mGy) with factors selected by iAEC	% change in dose if optimal factors used (compared to AEC selection)	Remedial dose level in NHSBSP protocol (mGy)
20	25	W/Rh	38	0.20	0.49	-59	1.0
30	25	W/Rh	64	0.35	0.66	-47	1.5
40	28	W/Rh	67	0.59	0.85	-30	2.0
45	25	W/Rh	123	0.78	0.96	-19	2.5
50	25	W/Rh	160	1.01	1.12	-10	3.0
60	25	W/Rh	235	1.64	1.46	12	4.5
70	25	W/Rh	362	2.65	1.93	37	6.5

3.9 Other tests

The results of all the other tests that were carried out were within acceptable limits as prescribed in the UK protocol and IPEM Report 89.[4]

3.9.1 Tube voltage

The tube voltage measurements are shown in Table 17. All were within 0.7kV of indicated values and compared favourably with the IPEM Report 89[4] remedial level of 1kV.

Table 17. Tube voltage measurements

Set voltage (kV)	Measured voltage (kV)
22	22.3
25	25.7
28	28.3
31	30.8
35	34.9

3.9.2 Compression

The measured compressed breast thicknesses are compared with the displayed values in Table 18. They were within 2mm of displayed values. This is well within the IPEM Report 89[4] remedial level of > 5mm.

Measurements of compression force together with the IPEM Report 89[4] remedial levels are shown in Table 19.

Table 18. Indicated compressed breast thickness

Field size (mm x mm)	Actual thickness (mm)	Indicated thickness (mm)	Difference (mm)
180 x 240	20	19	1
180 x 240	80	79	1
240 x 300	20	18	2
240 x 300	50	48	2
240 x 300	80	78	2

Table 19. Compression force

	Measured force (N)	IPEM Report 89 remedial level (N)
Difference between indicated and measured compression	4	> 20
Maximum motorised compression	198	< 150 or > 200
Maximum compression in any mode	238	> 300
Compression change over 30 seconds	3	> 20

3.9.3 Alignment

Alignment measurements for the 240mm x 300mm and 180mm x 240mm (central position) field sizes showed that the light field edges were all within 3mm of the edges of the radiation field (IPEM remedial level > 5mm). The radiation field overlapped the edges of the image by up to 2mm (remedial level < 0mm or > 5mm), except at the nipple edge for the 180mm x 240mm, where the overlap was 7mm.

3.9.4 Image retention

The image retention factor was 0.005, compared to the NHSBSP upper limit of 0.3.

3.9.5 Focal spot

The measured dimensions of the focal spot were 0.35mm x 0.35mm.

3.9.6 AEC repeatability

There was no variation in mAs for a series of 5 repeat images, which compared favourably with the NHSBSP remedial level of 5%. The variation in SNR was less than 1%.

3.9.7 Uniformity and artefacts

Uniformity measurements showed a variation in linearised pixel values of less than 6% relative to the central area. The NHSBSP remedial level is 10%. There were white unexposed borders up to 2mm deep at the chest wall and lateral edges of the QC images. There was also a very faint 12mm band along the CWE which represented a 2% reduction in sensitivity.

3.9.8 Cycle time

For a typical exposure of 29kV W/Rh at 64mAs, a subsequent exposure could be made 16 seconds after the start of the previous one.

3.9.9 Backup timer

When an AEC exposure was attempted with a steel plate blocking the X-ray beam and an indicated breast thickness of 224mm, the exposure terminated after a short time of less than a second following the pre-exposure. There was no main exposure and no image acquired, as confirmed by its values of 0kV and 0mAs in the DICOM image header, although the pre-exposure for the image was shown as 40kV and 60mAs in the DICOM header.

4. Discussion

The detector response was found to be logarithmic. This was as expected for Fujifilm systems.

MGDs measured using PMMA were well within the NHSBSP limits for all equivalent breast thicknesses at all three dose settings when using iAEC mode (Figure 5). The MGDs to a 53mm equivalent breast thickness were 1.03mGy, 0.61mGy and 1.48mGy at dose settings N, L and H respectively (Table 6). All these are well below the dose limit of 2.5mGy.

CNR measurements made with plain PMMA showed a marked decrease with increasing equivalent breast thickness.

Target CNR values of 3.8 and 5.7, for minimum acceptable and achievable image quality respectively, were calculated from the CNR and threshold gold thickness results.

At dose setting N in iAEC mode, the CNRs exceeded the target for the achievable level of image quality for equivalent breast thicknesses of up to 45mm. For a 90mm equivalent breast thickness, the CNR was midway between the minimum acceptable and achievable levels.

At dose setting H in iAEC mode, the CNR for a 90mm equivalent breast thickness approached the target level for achievable image quality. At dose setting L in iAEC mode, the target CNR for the achievable level of image quality was only met for equivalent breast thicknesses up to 32mm. In this dose setting, the CNR failed to reach the target for the minimum acceptable level of image quality for equivalent breast thicknesses of 75mm and 90mm (Figure 6).

The local dense area test showed that a nearly constant SNR (within 5%) was maintained with a local dense area within 60mm of the CWE, with the AEC operating in iAEC mode (Table 9). When the dense area was moved to 80mm from the CWE, it was apparently not detected and the SNR decreased by 50%. When the AEC operated in AEC mode, the SNR was maintained to within 22% (Table 10). These results show that there is an improvement in performance with the AEC in iAEC mode compared with AEC mode.

Noise analysis showed that quantum noise dominates the noise at the AEC operating level (Figure 10). There are minimal contributions from electronic and structural noise.

In iAEC mode, at dose setting N, with a selected dose of 1.12mGy for a 60mm standard breast, the image quality was close to the achievable level for all contrast detail diameters. The achievable level of image quality was exceeded for all detail diameters at a dose of 1.76mGy, which is close to the dose to a 60mm breast using iAEC mode at the H dose setting.

Threshold gold thickness measurements at different dose levels for the 0.1mm and 0.25mm diameter details were used to calculate MGDs to a simulated 60mm equivalent breast required for the minimum and achievable levels of image quality (Figure 13). The dose required for the Innovality to reach the achievable level of image quality was comparable to that measured for other digital mammography systems (Tables 13 and 14).

The optimisation tests suggest, surprisingly, that the optimum tube voltage for all PMMA thicknesses is 25 to 28kV (Figure 21). However, it may not be practical to reduce the kV for the larger thicknesses as this would require longer exposure times. To reach the

target CNR for the achievable level of image quality across all breast thicknesses, a decrease of approximately 60% in dose could be made for 20mm breasts, while the larger 90mm breasts would require a dose increase of at least 40% compared with that under iAEC (at dose setting N).

5. Conclusion

The Fujifilm AMULET Innovality meets the minimum requirements of the NHSBSP standards for digital mammography systems when operating with dose setting N in iAEC mode. The image quality exceeds the minimum acceptable level for all equivalent breast thicknesses up to 90mm.

Operating with dose setting L fails to meet the NHSBSP and European standards for image quality. It is, therefore, not recommended for use by the NHSBSP.

Ideally, the achievable level of image quality should be met for all breast thicknesses. With the AEC operating at dose setting N in iAEC mode, this is achieved for equivalent breast thicknesses up to 60mm (50mm PMMA). With the AEC at dose setting H, the achievable level of image quality is exceeded for breast thicknesses up to 75mm, and is almost met for the 90mm equivalent breast thickness. To reach the achievable level of image quality for the widest range of breast thicknesses, dose setting H in iAEC mode is recommended for use in the NHSBSP. In that mode, the dose to the standard breast is 1.48mGy, well below the dose limit of 2.5mGy.

Use of the iAEC mode with dose setting H is recommended to maintain good image quality within denser areas of the breast.

References

1. Kulama E, Burch A, Castellano I et al. *Commissioning and routine testing of full field digital mammography systems* (NHSBSP Equipment Report 0604, Version 3). Sheffield: NHS Cancer Screening Programmes, 2009

2. van Engen R, Young KC, Bosmans H, et al. European protocol for the quality control of the physical and technical aspects of mammography screening. In *European guidelines for quality assurance in breast cancer screening and diagnosis*, Fourth Edition. Luxembourg: European Commission, 2006

3. van Engen R, Bosmans H, Dance D et al. Digital mammography update: European protocol for the quality control of the physical and technical aspects of mammography screening. In *European guidelines for quality assurance in breast cancer screening and diagnosis,* Fourth edition – Supplements. Luxembourg: European Commission, 2013

4. Moore AC, Dance DR, Evans DS et al. *The Commissioning and Routine Testing of Mammographic X-ray Systems.* York: Institute of Physics and Engineering in Medicine, Report 89, 2005

5. Alsager A, Young KC, Oduko JM. Impact of heel effect and ROI size on the determination of contrast-to-noise ratio for digital mammography systems. In *Proceedings of SPIE Medical Imaging*, Bellingham WA: SPIE Publications, 2008, 691341: 1-11

6. Boone JM, Fewell TR and Jennings RJ. Molybdenum, rhodium and tungsten anode spectral models using interpolating polynomials with application to mammography. *Medical Physics*, 1997, 24: 1863-1974

7. Berger MJ, Hubbell JH, Seltzer SM, Chang et al. XCOM: Photon Cross Section Database (version 1.3) http://physics.nist.gov/xcom (Gaithersburg, MD, National Institute of Standards and Technology), 2005

8. Young KC, Oduko JM, Bosmans H, Nijs K, Martinez L. Optimal beam quality selection in digital mammography. *British Journal of Radiology*, 2006, 79: 981-990

9. Young KC, Cook JH, Oduko JM. Automated and human determination of threshold contrast for digital mammography systems. In *Proceedings of the 8th International Workshop on Digital Mammography,* Berlin: Springer-Verlag, 2006, 4046: 266-272

10. Young KC, Alsager A, Oduko JM et al. Evaluation of software for reading images of the CDMAM test object to assess digital mammography systems. In *Proceedings of SPIE Medical Imaging*, Bellingham WA: SPIE Publications, 2008, 69131C: 1-11

11. IEC 62220-1-2, *Determination of the detective quantum efficiency – Detectors used in mammography.* International Electrotechnical Commission, 2007

12. Young KC, Cook JJH, Oduko JM. Use of the European protocol to optimise a digital mammography system. In *Proceedings of the 8th International Workshop on Digital Mammography*, Berlin, Germany: Springer-Verlag, Lecture Notes in Computer Science, 2006, 4046:362-369

13. Young KC, Oduko JM. *Technical evaluation of the Hologic Selenia full field digital mammography system with a tungsten tube* (NHSBSP Equipment Report 0801). Sheffield: NHS Cancer Screening Programmes, 2008

14. Young KC, Oduko JM, Gundogdu O and Asad M. *Technical evaluation of profile automatic exposure control software on GE Essential FFDM systems* (NHSBSP Equipment Report 0903). Sheffield: NHS Cancer Screening Programmes, 2009

15. Young KC, Oduko JM and Asad M. *Technical Evaluation of Agfa DX-M Mammography CR Reader with HM5.0 Needle-IP* (NHSBSP Equipment Report 0905). Sheffield: NHS Cancer Screening Programmes, 2009

16. Young KC, Oduko JM, Gundogdu, O, Alsager, A. *Technical evaluation of Siemens Mammomat Inspiration Full Field Digital Mammography System* (NHSBSP Equipment Report 0909). Sheffield: NHS Cancer Screening Programmes, 2009

17. Young KC, Oduko JM. *Technical evaluation of Hologic Selenia Dimensions 2-D Digital Breast Imaging System with software version 1.4.2* (NHSBSP Equipment Report 1201). Sheffield: NHS Cancer Screening Programmes, 2012

18. Strudley CJ, Young KC, Oduko JM. *Technical Evaluation of the IMS Giotto 3DL Digital Breast Imaging System* (NHSBSP Equipment Report 1301). Sheffield: NHS Cancer Screening Programmes, 2013

19. Oduko JM, Young KC, Warren L. *Technical evaluation of the Fuji Amulet f/s Digital Breast Imaging System* (NHSBSP Equipment Report 1304). Sheffield: NHS Cancer Screening Programmes, 2013

20. Oduko JM, Young KC. *Technical evaluation of Philips MicroDose L30 with AEC software version 8.3* (NHSBSP Equipment Report 1305). Sheffield: NHS Cancer Screening Programmes, 2013